J. Fluid Mech. (1996), *vol.* 310, *pp.* 113–137

Unsteady transonic nozzle flow of dense gases

By A. KLUWICK AND ST. SCHEICHL

Institut für Strömungslehre und Wärmeübertragung, Technische Universität Wien, A-1040 Wien, Austria

(Received 14 February 1995 and in revised form 17 October 1995)

Vapours of retrograde fluids, i.e. media with large values of the specific heats, may have the remarkable property that sonic conditions are reached three times rather than once during isentropic expansion or compression. As a result, the acceleration of such a fluid through a converging–diverging Laval nozzle under steady flow conditions may lead to the occurrence of an expansion shock discontinuity. Theoretical considerations then suggest that nozzles with two throats should be designed to achieve a full shock-free subsonic–supersonic expansion.

In this study the unsteady flow of a dense, retrograde gas through slender nozzles (with one and two throats) is considered. The combination of the Navier–Stokes equations supplemented with a non-classical equation of state for the fluid yields a generalized wave equation, with its validity restricted to flow conditions near the critical value $M = 1$. This equation is used to study the transition process which sets in if a steady subsonic solution is perturbed by lowering the pressure at the end of the nozzle.

1. Introduction

Recent studies (e.g. Burnside 1973; Smith 1981; Curran 1981; Zörner & Blumenberg 1989) indicate that fluids having large specific heats may prove beneficial in Rankine power cycles if the maximum temperatures which can be achieved are relatively low as in the case of solar cycles, geothermal cycles, etc. These so-called retrograde fluids have the distinguishing property that the vapour dries rather than wets during isentropic expansion. Moreover, for even larger values of the specific heats the fundamental derivative

$$\Gamma := \frac{1}{\tilde{a}}\left(\frac{\partial(\tilde{\rho}\tilde{a})}{\partial\tilde{\rho}}\right)_{\tilde{s}},$$

which in the case of perfect gases and other regular fluids is a strictly positive quantity, is found to change sign and to become negative in the neighbourhood of the critical point. Here $\tilde{a}$, $\tilde{\rho}$ and $\tilde{s}$ denote the speed of sound, the density and the entropy, respectively.

The possibility that real fluids may exhibit regions of negative Γ in the dense-gas regime seems to have been recognized first by Bethe (1942) and independently by Zel'dovich (1946) on the basis of the Van der Waals equation of state. As an example, figure 1 shows the location of the transition line $\Gamma = 0$ in the pressure ($\tilde{p}$)–specific volume ($1/\tilde{\rho}$) plane for a Van der Waals fluid, assuming that the (constant) isochoric heat capacity $\tilde{c}_v$ is 50 times larger than the universal gas constant $\tilde{R}$, which roughly corresponds to n-octane. Using more refined and accurate equations of state, several members of the families of hydrocarbons and fluorocarbons were later identified as

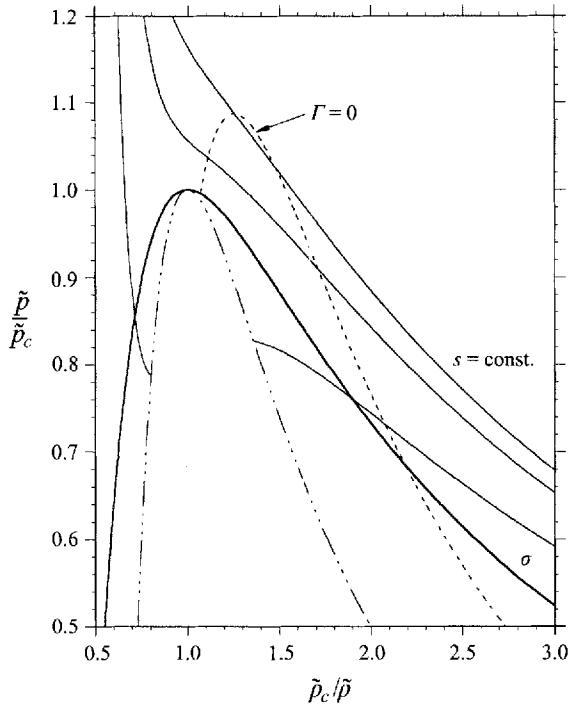

FIGURE 1. $(\tilde{p}, 1/\tilde{\rho})$-diagram of a Van der Waals gas with $\tilde{c}_v/\tilde{R} = 50$ showing regions of $\Gamma > 0$ and $\Gamma < 0$: ——, phase boundary; ——, isentropes; -----, transition line; —···—, spinodal lines.

candidates for real negative-Γ-fluids by Thompson and co-workers (e.g. Thompson 1971; Thompson & Lambrakis 1973). Because of the significance of each of these studies by Bethe, Zel'dovich and Thompson it has become common to refer to retrograde fluids that exhibit negative-Γ regions as BZT-fluids. Very recent calculations strongly point to the existence of silicon based BZT-fluids in addition to the hydrocarbons and fluorocarbons mentioned earlier (private communication by M. Cramer, see also Angelino & Invernizzi 1993).

Most studies of Rankine-cycle power systems using retrograde fluids or BZT-fluids as working media have concentrated so far on purely thermodynamic considerations, while gasdynamic aspects have received only very scant attention. However, a more complete evaluation of such systems will certainly have to take into account the unusual flow properties of these fluids, which include a number of new phenomena not encountered in classical gasdynamics (e.g. Cramer 1991; Kluwick 1991; Thompson 1991). As a first step steady external transonic flows of BZT-fluids were investigated by Cramer & Tarkenton (1992), while steady transonic nozzle flows were studied by Chandrasekar & Prasad (1991) and Kluwick (1993). Nozzle flows of retrograde and BZT-fluids with arbitrary large Mach number variation were computed numerically by Cramer & Fry (1993).

These studies have revealed a number of interesting new results. For example, it has been found that there exists a range of stagnation conditions for which the distributions of the field quantities on the axis of a conventional converging–diverging nozzle for subsonic flow reaching critical conditions at the throat and for subsonic–supersonic flow are different not only downstream, but also upstream of the throat (figure 2*b*). Moreover, a shock-free subsonic–supersonic expansion cannot be achieved by means of such a Laval nozzle for an even larger range of stagnation conditions. In order to

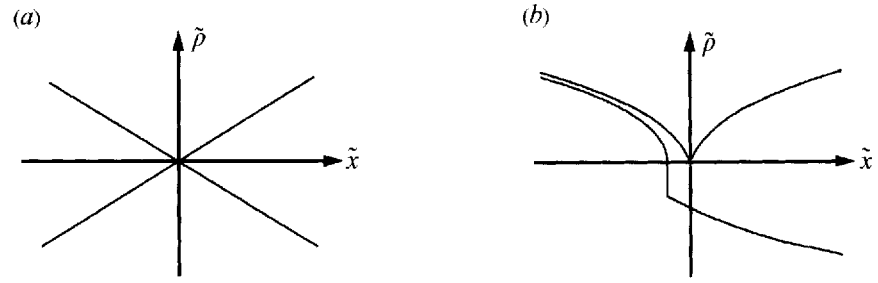

FIGURE 2. Density distributions (not to scale) in the throat area of a converging–diverging nozzle corresponding to accelerating–decelerating and purely accelerating flow. (*a*) Perfect gas, (*b*) BZT-fluid ($\hat{A}_0^2/3N_0 > \hat{\Gamma}_0 > 0$, $\hat{A}_0 > 0$).

avoid shocks nozzles with two throats, rather than a single throat, are required in these cases. The local Mach number then assumes its critical value of 1 in both throats and the intervening antithroat which reflects the fact that the Mach number–density relationship corresponding to these stagnation conditions exhibits three sonic points.

The results summarized so far naturally raise the question of whether and how a steady subsonic–supersonic expansion of a BZT-fluid can be achieved starting from subsonic conditions by, for example, lowering the exit pressure of the nozzle. The basic conceptual difficulty associated with such a transition process can be inferred most easily if the initial density distribution on the axis of a Laval nozzle is identified with the subsonic solution reaching a critical state at the throat. Since the density perturbations vary linearly with distance $\tilde{x}$ as $\tilde{x} \to 0+$, upstream-propagating waves cannot reach the throat $\tilde{x} = 0$ in a finite time. This is of no concern in the case of a perfect gas (figure 2*a*) as the density distribution upstream of the throat remains unchanged during the transition process leading from subsonic to subsonic–supersonic conditions. However, in the case of a BZT-fluid the density distribution there has to be modified also. A similar difficulty arises in the case of nozzles with two throats, where a solution with three sonic states has to be generated from a solution with a single sonic state. It is the aim of the present paper to investigate these starting problems in more detail. As in the study by Kluwick (1993, in the following referred to as I), the considerations will be limited to the throat area of the nozzle, where the flow is assumed to be transonic and quasi-one-dimensional.

The range of validity of the quasi-one-dimensional (hydraulic) approximation in the transonic regime has been studied extensively in the past for the perfect gas case (e.g. Ryzhov 1978; Adamson & Messiter 1988). If the wall curvature of the nozzle under consideration is small, the variations of the various field quantities in the lateral directions are small too, and, as demonstrated by Oswatitsch & Rothstein (1942) and independently by Szaniawski (1965), it is possible to construct series solutions containing powers of the transverse coordinate and functions of the distance along the centreline in which the quasi-one-dimensional result serves as the leading-order term. Using asymptotic methods, Adamson, Messiter & Richey (1974) and Messiter & Adamson (1975) have shown how these series solutions can be derived in a more systematic way and how they can be generalized to include unsteady effects. In addition, their analysis indicates that the series solutions are not uniformly valid if the quasi-one-dimensional approximation exhibits shock discontinuities or discontinuities of the first-order derivatives of the field quantities at the nozzle throat. In both cases the series solution plays the role of an outer solution which has to be supplemented with appropriate inner solutions holding in thin layers centred at shocks or the throat,

whose thickness tends to zero in the limit of vanishing wall curvature. As an example, it was shown that the (outer) series solution for accelerating–decelerating flow leading to critical conditions at the throat can be matched with an (inner) similarity solution of the full transonic nonlinear small-disturbance equation obtained by Tomotika & Tamada (1950). Unfortunately, however, the use of similarity solutions to render the series approximations uniformly valid turns out to be rather limited. Although such solutions can be derived for flows with shock discontinuities and unsteady flows (Ryzhov 1967; Adamson & Richey 1973), these solutions do in general not satisfy the requirements of steady nozzle geometry and smooth walls. As a result, the construction of appropriate inner solutions for such flows will require substantial numerical efforts. To the authors' knowledge systematic numerical studies of this problem have not been performed yet.

The general description of the flow structure in slender nozzles summarized so far carries over unchanged to the dense-gas regime where effects of negative nonlinearity come into play. Again, the quasi-one-dimensional solution – to be determined in this study – should be regarded as the leading-order term of an asymptotic outer solution. As in the perfect gas case, it is expected to capture the essential flow features.

2. Problem formulation

In this paper we consider the unsteady inviscid flow of a dense gas through a slender nozzle as sketched in figure 3. As in I it will be assumed that the nozzle shape is independent of the time $\tilde{t}$ and that the area of the cross-section $\tilde{A}(\tilde{x})$ changes sufficiently slowly with the distance $\tilde{x}$ so that the variations of the field quantities in the direction normal to the nozzle axis are negligibly small. Again, the investigations will be restricted to the throat region of the nozzle, where the Mach number M differs only slightly from the critical value $M = 1$.

Introducing the non-dimensional variables

$$\left.\begin{gathered} x = \frac{\tilde{x}}{\tilde{L}}, \quad t = \frac{\tilde{t}\tilde{a}_0}{\tilde{L}}, \quad A = \frac{\tilde{A}}{\tilde{A}_0}, \quad v = \frac{\tilde{v}}{\tilde{a}_0}, \quad W = \frac{\tilde{W}}{\tilde{a}_0}, \quad a = \frac{\tilde{a}}{\tilde{a}_0}, \quad \rho = \frac{\tilde{\rho}}{\tilde{\rho}_0}, \\ p = \frac{\tilde{p}}{\tilde{\rho}_0 \tilde{a}_0^2}, \quad s = \frac{\tilde{s}}{\tilde{c}_{v0}}, \quad h = \frac{\tilde{h}}{\tilde{a}_0^2}, \end{gathered}\right\} \tag{2.1}$$

the governing equations for inviscid unsteady quasi-one-dimensional flow can be written in the form

$$\frac{\partial \rho}{\partial t} + \frac{\partial(\rho v A)}{\partial x} = 0, \quad \frac{\partial v}{\partial t} + v\frac{\partial v}{\partial x} + \frac{1}{\rho}\frac{\partial p}{\partial x} = 0, \quad \frac{\partial s}{\partial t} + v\frac{\partial s}{\partial x} = 0. \tag{2.2}$$

Here $\tilde{v}$, $\tilde{\rho}$, $\tilde{p}$, $\tilde{T}$, $\tilde{h}$ and $\tilde{s}$ denote, respectively, the velocity, density, pressure, temperature, specific enthalpy and the entropy. The subscript 0 denotes quantities evaluated at a sonic reference state, $\tilde{L}$ and $\tilde{A}_0$ characterize the length and the cross-sectional area of the throat region and $\tilde{a} = (\partial\tilde{p}/\partial\tilde{\rho}|_{\tilde{s}})^{1/2}$ is the speed of sound.

It is convenient to cast the continuity, momentum and energy equations (2.2) into compatibility form:

$$\rho\frac{\mathrm{d}v}{\mathrm{d}t} \pm a\frac{\mathrm{d}\rho}{\mathrm{d}t} = \pm\left[\frac{av\rho(\mathrm{d}A/\mathrm{d}x)}{A} \pm \left(\frac{\partial p}{\partial s}\right)_\rho \frac{\partial s}{\partial x}\right] \quad \text{on} \quad \frac{\mathrm{d}x}{\mathrm{d}t} = v \pm a, \tag{2.3a, b}$$

$$\frac{\mathrm{d}s}{\mathrm{d}t} = 0 \quad \text{on} \quad \frac{\mathrm{d}x}{\mathrm{d}t} = v. \tag{2.4}$$

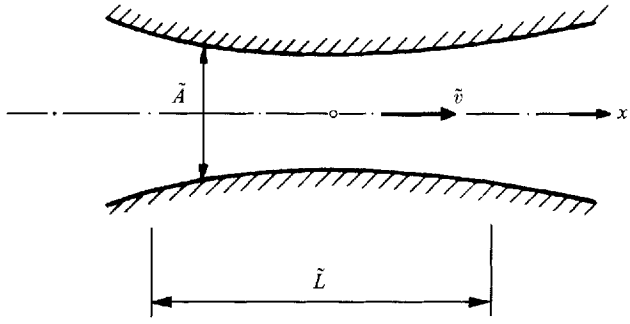

FIGURE 3. Sketch showing nozzle geometry and notation.

These relations have to be supplemented with the shock jump conditions

$$W[\rho] = [v\rho], \quad (W-v_b)(W-v_a) = \frac{[p]}{[\rho]}, \tag{2.5a, b}$$

$$[h] = \frac{1}{2}\left(\frac{1}{\rho_b}+\frac{1}{\rho_a}\right)[p], \quad [s] \geqslant 0, \tag{2.5c, d}$$

where W is the shock propagation speed. The square brackets denote the jumps of the quantities, i.e. $[Q] = Q_a - Q_b$ and the subscripts a and b refer to conditions after and before the shock.

In this study we are concerned with the evolution of disturbances generated downstream of the throat area. Appropriate initial and boundary conditions then are

$$t = 0, \forall x: \quad \rho = \rho_i(x), \quad p = p_i(x), \quad v = v_i(x); \tag{2.6a}$$

$$t > 0, x = x_0: \quad p = p_i(x_0) + p'(t); \tag{2.6b}$$

$$t > 0, x \to -\infty: \quad \partial\rho/\partial t = \partial p/\partial t = \partial v/\partial t = 0. \tag{2.6c}$$

Specifically, it will be assumed that the initial data correspond to a steady-state solution of equations (2.3*a, b*) and (2.4). The function $p'(t)$ characterizes the pressure disturbances imposed at a fixed distance x_0 downstream of the throat region.

3. Unsteady transonic small-perturbation equation

As pointed out earlier, BZT-fluids are characterized by the existence of isentropes on which sonic conditions may be reached three times rather than once during expansion or compression. In general, the corresponding values of the density ρ_1^*, ρ_2^*, ρ_3^* are well spaced, i.e. $(\rho_1^*-\rho_2^*)/\rho_1^* = O(1)$, $(\rho_1^*-\rho_3^*)/\rho_1^* = O(1)$, necessitating a numerical treatment of the nozzle flow problem as in the case of steady flow investigated by Cramer & Fry (1993). If, however, the reference state is in the vicinity of the point in the $(p, 1/\rho)$-diagram where the isentrope touches the transition line, Γ and $\partial\Gamma/\partial\rho|_s$ are small and so are the differences between the critical values of the densities, thus allowing a perturbation approach, see I.

3.1. *Small-disturbance approximation*

Let $\epsilon \ll 1$ be a measure of the small density disturbances inside the throat area. Then ρ is expressed in the form

$$\rho = 1 + \epsilon\rho_1 + \epsilon^2\rho_2 + \epsilon^3\rho_3 + o(\epsilon^3). \tag{3.1}$$

Owing to the requirement imposed on the reference state, Γ and its first and second derivative with respect to the density satisfy the order of magnitude relationships

$$\left.\begin{aligned} \Gamma(1,s_0) &= \epsilon^2\hat{\Gamma}_0, \quad \hat{\Gamma} = O(1), \\ \frac{\partial\Gamma}{\partial\rho}(1,s_0) &= \epsilon\hat{A}_0, \quad \hat{A}_0 = O(1), \\ \frac{\partial^2\Gamma}{\partial\rho^2}(1,s_0) &= N_0, \quad N_0 = O(1). \end{aligned}\right\} \tag{3.2}$$

As shown in Cramer & Crickenberger (1991) and I, the entropy jump across weak shocks is of fifth order in ϵ:

$$s = 1+\epsilon^5 s_5 + o(\epsilon^5). \tag{3.3}$$

According to (3.1), (3.2) and (3.3) the leading-order term of the expansion for Γ is given by

$$\Gamma = \epsilon^2\hat{\Gamma}+o(\epsilon^2), \quad \hat{\Gamma} = \hat{\Gamma}_0+\hat{A}_0\rho_1+\tfrac{1}{2}N_0\rho_1^2. \tag{3.4}$$

By using standard thermodynamic relationships the following expansions for p and a can be derived:

$$p = 1+\epsilon p_1+\epsilon^2 p_2+\epsilon^3 p_3+o(\epsilon^3) = 1+\epsilon\rho_1+\epsilon^2(-\rho_1^2+\rho_2)+\epsilon^3(\rho_1^3-2\rho_1\rho_2+\rho_3)+o(\epsilon^3), \tag{3.5}$$

$$a = 1-\epsilon\rho_1+\epsilon^2(\rho_1^2-\rho_2)+\epsilon^3\left((\tfrac{1}{6}N_0-1)\rho_1^3+\tfrac{1}{2}\rho_1^2\hat{A}_0+\hat{\Gamma}_0\rho_1+2\rho_1\rho_2-\rho_3\right)+o(\epsilon^3). \tag{3.6}$$

Furthermore, the leading-order term in the expansion for T is given by

$$T = 1+\epsilon\frac{\tilde{\beta}_0\tilde{a}_0^2}{\tilde{c}_{p0}}\rho_1+o(\epsilon), \tag{3.7}$$

with $\tilde{c}_p$ and $\tilde{\beta}$ representing, respectively, the isobaric heat capacity and the coefficient of thermal expansion.

3.2. *Evolution equation*

Similar to ρ and p, the velocity v is also expanded in the form

$$v = 1+\epsilon v_1+\epsilon^2 v_2+\epsilon^3 v_3+o(\epsilon^3). \tag{3.8}$$

If the effects of the changing area of cross-section and the time are to be retained at the appropriate levels of approximation, we have to write

$$A = 1+\epsilon^4 A_4+o(\epsilon^4) \tag{3.9}$$

and to require that the various field quantities depend on x and the slow time

$$\hat{t} = \epsilon^3 t. \tag{3.10}$$

Here the scaling of t depends crucially on the assumption made in §2 that no disturbances enter the throat from upstream. As will be shown later, the speed of upstream-propagating waves then is of $O(\epsilon^3)$ and (3.10), therefore, reflects the fact that the time needed for an upstream-propagating wave to transverse the throat region is of $O(1/\epsilon^3)$.

Substitution of the expansions (3.1), (3.2), (3.3), (3.5), (3.6) and (3.8) into the compatibility condition (2.3*a*) for right-running characteristics leads to a set of perturbation equations, which can be solved in closed form. Taking into account the boundary conditions (2.6*c*) for $x\to-\infty$ one obtains

$$v_1 = -\rho_1, \quad v_2 = -\rho_2+\rho_1^2, \quad v_3 = -\rho_3-\rho_1^3+2\rho_1\rho_2. \tag{3.11a–c}$$

On substitution of the expansions (3.1), (3.2), (3.3), (3.5), (3.6) and (3.8) into the compatibility condition (2.3*b*) holding on left-running characteristics one obtains

$$\frac{\mathrm{d}v_1}{\mathrm{d}\hat{t}}-\frac{\mathrm{d}\rho_1}{\mathrm{d}\hat{t}}=-\frac{\mathrm{d}A_4}{\mathrm{d}x} \tag{3.12}$$

on

$$\frac{\mathrm{d}x}{\mathrm{d}\hat{t}}=v_3-((\tfrac{1}{6}N_0-1)\rho_1^3+\tfrac{1}{2}\rho_1^2\hat{A}_0+\hat{\Gamma}_0\rho_1+2\rho_1\rho_2-\rho_3). \tag{3.13}$$

Combination of (3.11), (3.12) and (3.13) yields the single evolution equation for ρ_1:

$$\frac{\partial\rho_1}{\partial\hat{t}}-(\hat{\Gamma}_0\rho_1+\tfrac{1}{2}\hat{A}_0\rho_1^2+\tfrac{1}{6}N_0\rho_1^3)\frac{\partial\rho_1}{\partial x}=-\frac{1}{2}\frac{\mathrm{d}A_4}{\mathrm{d}x}. \tag{3.14}$$

Introducing the perturbation mass flux density

$$j_1=-\hat{\Gamma}_0\rho_1^2-\tfrac{1}{3}\hat{A}_0\rho_1^3-\tfrac{1}{12}N_0\rho_1^4, \tag{3.15}$$

the modified unsteady small-perturbation equation (3.14) can be written as

$$\frac{\partial\rho_1}{\partial\hat{t}}+\frac{1}{2}\frac{\partial j_1}{\partial x}=-\frac{1}{2}\frac{\mathrm{d}A_4}{\mathrm{d}x}. \tag{3.16}$$

Owing to the upstream boundary condition (2.6*c*), v_1, v_2, v_3 and ρ_1, ρ_2, ρ_3 are related in exactly the same way as in the case of a steady flow. As a consequence, the result

$$M-1=\frac{\epsilon^3}{2}\frac{\mathrm{d}j_1}{\mathrm{d}\rho_1} \tag{3.17}$$

derived in I for steady nozzle flow carries over unchanged to unsteady problems. Furthermore, the values of the density perturbations at sonic conditions $M=1$,

$$\rho_{1,1}^*=0 \tag{3.18}$$

and

$$\rho_{1,2/3}^*=-\frac{3\hat{A}_0}{2N_0}\left[1\pm\left(1-\frac{8\hat{\Gamma}_0N_0}{3\hat{A}_0^2}\right)^{1/2}\right] \quad \text{if} \quad \hat{\Gamma}_0\leqslant\frac{3\hat{A}_0^2}{8N_0}, \tag{3.19}$$

again correspond to the values of ρ_1 at the maxima and minima of the perturbation mass density $j_1(\rho_1)$.

Combination of (3.4) and (3.15) yields $\hat{\Gamma}=-\frac{1}{2}\mathrm{d}^2j_1/\mathrm{d}\rho_1^2$. Accordingly, the local value of the fundamental derivative changes sign at the values of ρ_1 defined by the inflexion points of the (j_1,ρ_1)-diagram (figure 4).

3.3. *Formal solution of the evolution equation*

Substitution of (3.11*c*) into (3.13) which determines the propagation speed of left-running characteristics, labelled $\xi=\text{const.}$, yields

$$\left.\frac{\mathrm{d}x}{\mathrm{d}\hat{t}}\right|_\xi=-(\hat{\Gamma}_0\rho_1+\tfrac{1}{2}\hat{A}_0\rho_1^2+\tfrac{1}{6}N_0\rho_1^3)=\frac{1}{2}\frac{\mathrm{d}j_1}{\mathrm{d}\rho_1}. \tag{3.20}$$

As a consequence, the evolution equation (3.14) can be written in the equivalent form

$$\left.\frac{\mathrm{d}\rho_1}{\mathrm{d}\hat{t}}\right|_\xi=-\frac{1}{2}\frac{\mathrm{d}A_4}{\mathrm{d}x} \quad \text{or} \quad \frac{\mathrm{d}}{\mathrm{d}x}(j_1+A_4)|_\xi=0. \tag{3.21a, b}$$

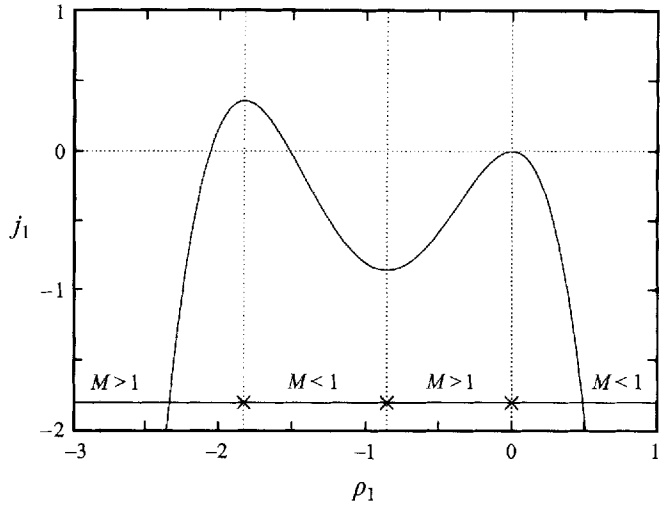

FIGURE 4. (j_1, ρ_1)-diagram for $\hat{A}_0^2/3N_0 > \hat{\Gamma}_0 > 0$, $\hat{A}_0 > 0$ ($\hat{\Gamma}_0 = 4.6$, $\hat{A}_0 = 15.8$, $N_0 = 17.67$).

A formal solution of this equation is given by

$$j_1(\rho_1(x,\xi)) + A_4(x) = f(\xi), \tag{3.22}$$

where $f(\xi)$ is an arbitrary function.

It is interesting to note that (3.22) differs from its steady counterpart

$$j_1(\rho_1(x)) + A_4(x) = Q \tag{3.23}$$

derived in I only insofar as the integration constant Q is replaced with the function $f(\xi)$. On each characteristic $\xi = \text{const.}$, therefore, j_1 and A_4 are related in exactly the same way as in the case of steady flow. Similar to the case of steady flow, (3.21) thus leads, in general, to the occurrence of regions of multivaluedness, which have to be obviated by the insertion of shock fronts. In contrast to steady nozzle flow, however, these shocks may generate extra characteristics if the upstream or/and downstream state is sonic.

3.4. *Weak thermoviscous effects*

So far the considerations have been limited to inviscid flows. Weak thermoviscous effects, however, can be easily incorporated into the analysis. To this end, we assume, following I, that the Reynolds number based on the characteristic wavelength is large:

$$Re = \frac{\tilde{a}_0 \tilde{L} \tilde{\rho}_0}{\tilde{\mu}_0} = O(\epsilon^{-3}). \tag{3.24}$$

The appropriate generalization of (3.16) then is found to be

$$\frac{\partial \rho_1}{\partial \hat{t}} + \frac{1}{2}\frac{\partial j_1^{inv}}{\partial x} = -\frac{1}{2}\frac{\mathrm{d}A_4}{\mathrm{d}x} + \frac{1}{2}\delta_0 \frac{\partial^2 \rho_1}{\partial x^2}. \tag{3.25}$$

Here the abbreviation *inv* characterizes the inviscid part of the mass flux density still defined by (3.15), δ_0 is the acoustic diffusivity of a general fluid (e.g. Cramer & Kluwick 1984)

$$\delta_0 = \frac{1}{\epsilon^3 Re}\left(\frac{\tilde{\lambda}_0}{\tilde{\mu}_0} + 2 + \frac{\tilde{\beta}_0^2 \tilde{T}_0 a_0^2}{Pr\, \hat{c}_{p0}}\right), \tag{3.26}$$

and $\tilde{\lambda}_0$, $\tilde{\mu}_0$, $\tilde{\beta}_0$ and Pr denote, respectively, the first and second viscosity, the coefficient of thermal expansion and the Prandtl number evaluated at the unperturbed state.

4. Weak shocks

4.1. *Shock propagation speed*

Assuming as before that the area of cross-section A_4 varies continuously with x, the shock propagation speed

$$\hat{W} = \frac{\mathrm{d}x_s}{\mathrm{d}\hat{t}} \tag{4.1}$$

is expanded as $$\hat{W} = \frac{1}{\epsilon^3}(1 + \epsilon W_1 + \epsilon^2 W_2 + \epsilon^3 W_3 + o(\epsilon^3)). \tag{4.2}$$

Straightforward manipulation of the shock jump conditions then yields $W_1 = W_2 = 0$, as expected, and

$$\hat{W} = -\tfrac{1}{2}\hat{\Gamma}_0(\rho_{1b} + \rho_{1a}) - \tfrac{1}{6}\hat{\Lambda}_0(\rho_{1b}^2 + \rho_{1b}\rho_{1a} + \rho_{1a}^2) - \tfrac{1}{24}N_0(\rho_{1b}^3 + \rho_{1b}^2\rho_{1a} + \rho_{1b}\rho_{1a}^2 + \rho_{1b}^3). \tag{4.3}$$

Using the definitions of the perturbation mass flux density (3.15), the leading-order approximation to (4.1) thus assumes the form

$$\hat{W} = \frac{\mathrm{d}x_s}{\mathrm{d}\hat{t}} = \frac{1}{2}\frac{[j_1]}{[\rho_1]} \tag{4.4}$$

typical for all kinematic wave theories, e.g. Whitham (1974).

4.2. *Shock admissibility criteria*

As shown in I, the entropy jump across weak shocks having $\Gamma_b = O(\epsilon^2)$, $\Lambda_b = O(\epsilon)$, $N_b = O(1)$ can be calculated from the relationship

$$\frac{\hat{c}_{v0}\tilde{T}_0}{\tilde{a}_0^2}[s] = \tfrac{1}{6}\epsilon^5[\rho_1]^3\{\hat{\Gamma}_0 + \tfrac{1}{2}\hat{\Lambda}_0(\rho_{1a} + \rho_{1b}) + \tfrac{1}{20}N_0(3\rho_{1a}^2 + 4\rho_{1a}\rho_{1b} + 3\rho_{1b}^2)\} + o(\epsilon^5). \tag{4.5}$$

Similar to the case of a steady flow, the requirement $[s] \geqslant 0$ following from the second law of thermodynamics is not strong enough to rule out inadmissible shocks, i.e. shocks for which a thermoviscous profile does not exist. In order to derive the additional conditions which have to be met by admissible shocks it is necessary to carry out a matched asymptotic analysis of the modified viscous transonic small-perturbation equation (3.25) in the limit $\delta_0 \to 0$. The (inner) structure problem then is formulated in terms of the stretched variables

$$\bar{x} = \frac{x - x_s(\hat{t})}{\delta_0}, \quad \bar{t} = \hat{t}, \tag{4.6}$$

where $x_s(\hat{t})$ denotes the shock path occurring in the (outer) inviscid solution.

Substitution of the definitions (4.6) into (3.25) yields for $\delta_0 \to 0$

$$\left(\frac{1}{2}\frac{\mathrm{d}j_1}{\mathrm{d}\rho_1} - \hat{W}\right)\frac{\partial\rho_1}{\partial\bar{x}} = \frac{\partial^2\rho_1}{\partial\bar{x}^2}, \tag{4.7}$$

which has to be solved subject to the boundary conditions

$$\rho_1|_{\bar{x}\to-\infty} \to \rho_{1b}, \quad \rho_1|_{\bar{x}\to\infty} \to \rho_{1a}, \tag{4.8}$$

following from the match with the inviscid flow outside the shock layer.

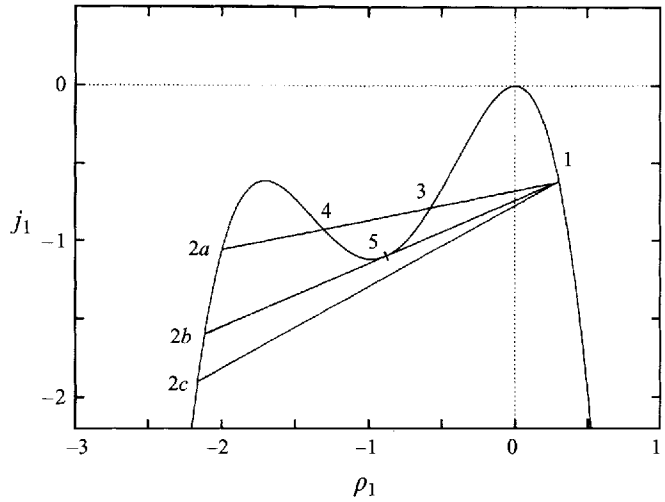

FIGURE 5. (j_1,ρ_1)-diagram for $3\hat{A}_0^2/8N_0 > \hat{\Gamma}_0 > \hat{A}_0^2/3N_0$, $\hat{A}_0 > 0$ ($\hat{\Gamma}_0 = 4.91$, $\hat{A}_0 = 15.8$, $N_0 = 17.67$) including Rayleigh lines of admissible shocks (e.g. $1 \to 3$, $4 \to 2a$, $4 \to 3$, $1 \to 2b$) and inadmissible shocks (e.g. $2a \to 1$, $3 \to 4$, $3 \to 1$, $5 \to 1$).

The structure problem (4.7), (4.8) is of exactly the same form as the set of equations derived by Cramer & Crickenberger (1992) for the case of one-dimensional weakly onlinear waves. As a result, we obtain

$$\text{the shock admissibility criterion A (figure 5)} \begin{cases} \text{the Rayleigh line connecting} \\ \text{the values of } \rho_1 \text{ before} \\ \text{and after the shock must not} \\ \text{cut intervening branches of} \\ \text{the } (j_1,\rho_1)\text{-diagram;} \end{cases} \quad (4.9)$$

$$\left.\frac{\mathrm{d}x}{\mathrm{d}\hat{t}}\right|_b \geqslant \hat{W} \geqslant \left.\frac{\mathrm{d}x}{\mathrm{d}\hat{t}}\right|_a .$$

Taking into account that for each fixed value of $\hat{t}$ there exists a functional relationship between j_1 and x, once the function $f(\xi)$ entering equation (3.22) has been specified, this result can be expressed in the form of

$$\text{the shock admissibility criterion B} \begin{cases} \text{the line } x = \text{ const. connecting the} \\ \text{values of } \rho_1 \text{ before and after the} \\ \text{shock must not cut intervening} \\ \text{branches of the density distribution;} \end{cases} \quad (4.10)$$

$$\left.\frac{\mathrm{d}x}{\mathrm{d}\hat{t}}\right|_b \geqslant \hat{W} \geqslant \left.\frac{\mathrm{d}x}{\mathrm{d}\hat{t}}\right|_a .$$

4.3. *Admissible and inadmissible shocks in the* (ρ_{1a},ρ_{1b})*-plane*

In order to decide whether a given pair of density perturbations (ρ_{1a},ρ_{1b}) meets or violates the shock admissibility criterion A it is necessary to investigate the roots of the quadratic equation

$$\tfrac{1}{24}N_0\rho_1^2 + (\tfrac{1}{6}\hat{A}_0 + \tfrac{1}{24}N_0(\rho_{1b}+\rho_{1a}))\rho_1 + (\tfrac{1}{2}\hat{\Gamma}_0 + \tfrac{1}{6}\hat{A}_0(\rho_{1b}+\rho_{1a}) + \tfrac{1}{24}N_0(\rho_{1b}^2+\rho_{1b}\rho_{1a}+\rho_{1a}^2)) = 0, \quad (4.11)$$

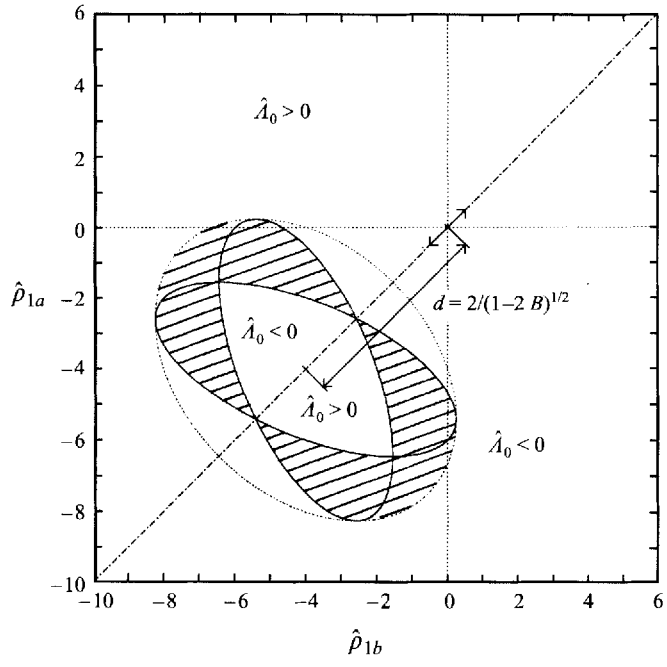

FIGURE 6. Admissible and inadmissible shocks in the $(\hat{\rho}_a, \hat{\rho}_b)$-plane. Density pairs violating the first part of criterion A are located within the hatched regions. In order to be able to meet the second part of criterion A regions representing admissible combinations are labelled according to the sign of $\hat{\Lambda}_0$.

which determine the intersection points $\rho_1 = \rho_{1c}, \rho_1 = \rho_{1d}$ between the Rayleigh line and intervening branches of the (j_1, ρ_1)-diagram. (See figure 5 for possible cases of pairs (ρ_{1a}, ρ_{1b}) with ρ_{1c}, ρ_{1d} being real or complex.)

If the parameter

$$B = \hat{\Gamma}_0 N_0 / \hat{\Lambda}_0^2 \tag{4.12}$$

is larger than $\frac{1}{2}$, the (j_1, ρ_1)-diagram exhibits a single extremum at $\rho_1 = \rho_1^* = 0$. As a result, all pairs (ρ_{1a}, ρ_{1b}) satisfy the first part of shock admissibility criterion A. However, by applying the wave speed ordering relationship it is easily shown that for $N_0 > 0$, which is of relevance here, shocks can occur in the form of compression shocks only.

If B is smaller than $\frac{1}{2}$, the following limiting cases have to be distinguished:

(i) $\rho_{1c} = \rho_{1d}$: the Rayleigh line touches the (j_1, ρ_1)-plot in an interior point,

(ii) $\rho_{1c} = \rho_{1b}$ or $\rho_{1d} = \rho_{1b}$: the shock has an upstream sonic state,

(iii) $\rho_{1c} = \rho_{1a}$ or $\rho_{1d} = \rho_{1a}$: the shock has a downstream sonic state.

The final results are expressed most conveniently in terms of the scaled density perturbations

$$\hat{\rho}_1 = \rho_1 \frac{N_0}{\hat{\Lambda}_0 (\frac{1}{2} - B)^{1/2}}, \quad B < \tfrac{1}{2}. \tag{4.13}$$

Pairs $(\hat{\rho}_{1a}, \hat{\rho}_{1b})$ for which conditions (i), (ii) or (iii) are satisfied are found to be located on ellipses centred at $\rho_{1a} = \rho_{1b} = -[2/(1-2B)]^{1/2}$ in the $(\hat{\rho}_{1a}, \hat{\rho}_{1b})$-plane (figure 6). The lengths a, b of their main axes and the inclination angle with respect to the $\hat{\rho}_{1b}$-axis are

$$\text{(i)}\quad a = 2\sqrt{3}, b = 2\sqrt{6}, \quad \alpha = -\tfrac{1}{4}\pi, \tag{4.14a}$$

$$\text{(ii)}\quad a = \left(\frac{6(2-\sqrt{2})}{3-2\sqrt{2}}\right)^{1/2}, \quad b = [6(2-\sqrt{2})]^{1/2}, \quad \alpha = -\tfrac{1}{8}\pi, \tag{4.14b}$$

$$\text{(iii)}\quad a = \left(\frac{6(2-\sqrt{2})}{3-2\sqrt{2}}\right)^{1/2}, \quad b = [6(2-\sqrt{2})]^{1/2}, \quad \alpha = -\tfrac{3}{8}\pi. \tag{4.14c}$$

5. Results

The results summarized so far are sufficient to solve the initial value problem formulated in §2. If shocks form, their position can be calculated from (4.4) in combination with the shock admissibility criteria (4.9) or (4.10).

In all cases treated here the shock path in the $(x, \hat{t})$-plane had to be determined numerically. To this end the shock speed at time $\hat{t}$ say was calculated from (4.4), inserting the density perturbations carried by the merging characteristics to obtain the approximate shock location at the slightly larger time $\hat{t}+\Delta\hat{t}$. If the shock at $\hat{t}+\Delta\hat{t}$ had a supersonic upstream and a subsonic downstream state the procedure was advanced to the next time step. If, however, the shock was found to have a sonic upstream or/and downstream state, additional characteristics had to be inserted to provide the correct density distribution inside regions of the $(x, \hat{t})$-plane which are inaccessible for characteristics emanating from the boundaries of the computational domain.

If the transition process considered led to the occurrence of a single shock, its position was checked independently by applying a global mass balance. To this end (3.16) was integrated with respect to x and $\hat{t}$ in the domain $x_1 \leqslant x \leqslant x_2$, $0 \leqslant \hat{t} \leqslant \hat{t}_1$. Under the assumption that the flow quantities at the upstream boundary $x = x_1$ remain constant (which for finite values of $\hat{t}_1$ can always be satisfied by an appropriate choice of x_1) one obtains the condition

$$\int_{x_1}^{x_s} \rho_1(x, \hat{t}_1)\,\mathrm{d}x + \int_{x_s}^{x_2} \rho_1(x, \hat{t}_1)\,\mathrm{d}x = \int_{x_1}^{x_2} \rho_1(x, 0)\,\mathrm{d}x - \frac{1}{2}\int_0^{\hat{t}_1} j_1(x_2, \hat{\tau})\,\mathrm{d}\hat{\tau} + \tfrac{1}{2}(j_1(x_1, \hat{t}) - A_4(x_2) + A_4(x_1))\,\hat{t}_1, \tag{5.1}$$

which yields the shock position x_s at time $\hat{t}_i$ provided that the density distribution $\rho_1(x, \hat{t}_1)$ is known.

5.1. *Laval nozzle: perfect gas*

Steady and unsteady transonic nozzle flows of perfect gases have been studied intensively in the past (e.g. Ryzhov 1978; Adamson & Messiter 1988). Nevertheless, it is useful to treat first the more simple perfect gas case of the start problem (2.6), which has been investigated earlier by Kluwick (1972) applying a different (inverse) method. The relevant relationships then follow from (3.15), (3.20) and (3.22) with the substitutions $\hat{\Gamma}_0 = (\gamma+1)/2$, $\hat{A}_0 = N_0 = 0$, $\hat{t} = \epsilon t$, $A_4 = (A-1)/\epsilon^2$, where γ denotes the ratio of the specific heats.

Specifically, it will be assumed that the shape of the classical convergent–divergent Laval nozzle in the region of interest is given by

$$A_4 = cx^2, \quad c > 0 \tag{5.2}$$

and that the initially imposed density distribution is subsonic with $M = 1$ at the throat $x = 0$:

$$\rho_1(x,0) = \rho_1^{sub}(x) = |x|\left(\frac{c}{\hat{\Gamma}_0}\right)^{1/2}. \tag{5.3}$$

The boundary condition at $x = x_0$ is written in the form

$$\rho_1(x_0,\hat{t}) = \rho_1^{sub}(x_0) + h(\hat{t}) \tag{5.4}$$

with

$$h(0) = 0, \quad h(\hat{t}) \leqslant 0, \quad \frac{\mathrm{d}h(\hat{t})}{\mathrm{d}\hat{t}} \leqslant 0 \quad \text{for} \quad \hat{T} \geqslant \hat{t} \geqslant 0. \tag{5.5}$$

Here $\hat{T}$ characterizes the time at which the imposed density reduction leads to the occurrence of the sonic state $\rho_1(x_0,\hat{T}) = 0$, and thus satisfies $h(\hat{T}) = -\rho_1^{sub}(x_0)$.

For $\hat{t} > \hat{T}$ the propagation speed of characteristics $\xi = \text{const.}$ at $x = x_0$ is positive and for simplicity the function $h(\hat{t})$ is chosen such that the imposed density perturbations (5.4) agree with the density perturbations carried by these characteristics as they leave the computational domain. In this way the necessary condition that $\rho_1(x_0,\hat{t})$ eventually assumes the value $-\rho_1^{sub}(x_0)$ characterizing the steady accelerating solution is satisfied automatically. Of course, any other form of $h(\hat{t})$ compatible with this requirement can be prescribed for $\hat{t} > \hat{T}$ in principle but generates shock waves which originate at the downstream boundary and obscure the basic features of the transition process of interest here.

From (3.22), (5.2), (5.3) and (5.4) the formal solution of the compatibility condition for $x \geqslant 0$ is found to be

$$\rho_1(x,\xi) = \pm\left[\frac{cx^2}{\hat{\Gamma}_0} + 2h(\xi)\rho_1^{sub}(x_0) + h(\xi)^2\right]^{1/2}, \quad \xi \geqslant 0, \tag{5.6a}$$

$$\rho_1(x,\xi) = \rho_1^{sub}(x), \quad \xi < 0. \tag{5.6b}$$

Herein, the parameterization

$$x = x_0: \quad \hat{t} = \xi \tag{5.7}$$

has been adopted without loss of generality.

Evaluation of equation (5.6*a*) for $\rho_1 = 0$ yields the representation

$$x^*(\xi) = \left[\frac{-\hat{\Gamma}_0}{c}(h(\xi)^2 + 2h(\xi)\rho_1^{sub}(x_0))\right]^{1/2} \tag{5.8}$$

for the x-location of the unsteady sonic line, along which solutions (5.6*a*) with different sign can be patched. Using this relationship, the solution of compatibility condition (5.6*a*) is written in the more compact form

$$\rho_1(x,\xi) = \pm\left[\frac{c}{\hat{\Gamma}_0}(x^2 - x^*(\xi)^2)\right]^{1/2}. \tag{5.9}$$

By integrating the slope condition

$$\frac{\mathrm{d}x}{\mathrm{d}\hat{t}} = -\hat{\Gamma}_0\rho_1 \tag{5.10}$$

one then obtains

$$\hat{t}(x,\xi) = \xi + \frac{2}{(\hat{\Gamma}_0 c)^{1/2}}\operatorname{artanh}\left(\frac{x_0 - x^*(\xi)}{x_0 + x^*(\xi)}\right)^{1/2} \mp \frac{2}{(\hat{\Gamma}_0 c)^{1/2}}\operatorname{artanh}\left(\frac{x - x^*(\xi)}{x + x^*(\xi)}\right)^{1/2}, \quad \xi \geqslant 0. \tag{5.11}$$

Identification of x and x^* leads to the result

$$\hat{t}^*(\xi) = \xi + \frac{2}{(\hat{\Gamma}_0 c)^{1/2}}\operatorname{artanh}\left(\frac{x_0 - x^*(\xi)}{x_0 + x^*(\xi)}\right)^{1/2}, \tag{5.12}$$

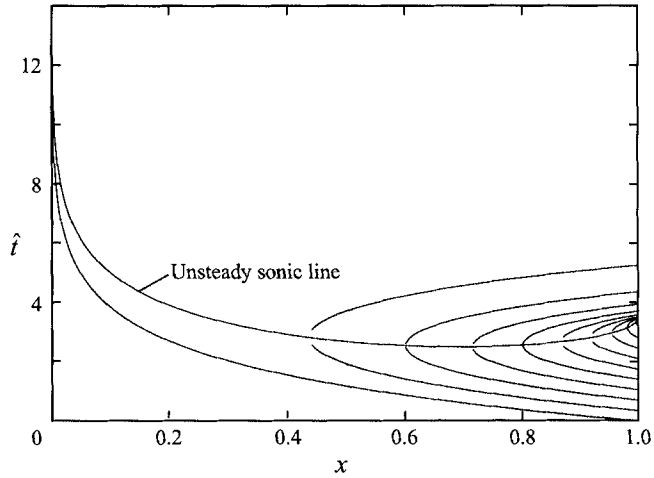

FIGURE 7. Laval nozzle: perfect gas ($\hat{\Gamma}_0 = 1.2$, $c = 0.3$, $x_0 = 1$, $\hat{T} = 3.5 > \rho_1^{sub}(x_0)/cx_0 = 1.667$). Position of characteristic curves and unsteady sonic line in the $(x, \hat{t})$-plane.

which together with (5.8) determines the position of the unsteady sonic line as a function of time.

To study the behaviour of this sonic line in the vicinity of the throat (5.12) is expanded for $x^*(\xi) \to 0$. To leading order one then obtains the explicit relationship

$$\frac{x^*(\hat{t})}{x_0} \sim 2\exp[-\hat{t}(\hat{\Gamma}_0 c)^{1/2}]. \tag{5.13}$$

It thus follows that – independent of the special choice of function $h(\xi)$ – the unsteady sonic line generated by the imposed density/pressure reduction at $x = x_0$ does not reach the throat $x = 0$ in finite time. As a consequence, the flow properties in the converging part of the nozzle $x < 0$ remain unaffected by the downstream boundary conditions at all times.

Differentiation of (5.8) and (5.12) with respect to ξ shows that the slope of the unsteady sonic line in the $(x, \hat{t})$-plane is given by

$$\frac{\mathrm{d}\hat{t}^*}{\mathrm{d}x} = -\frac{x_0 h'(\xi) + cx^*(\xi)^2}{x^*(\xi)(\hat{\Gamma}_0 c)^{1/2}(x_0^2 - x^*(\xi)^2)h'(\xi)}, \tag{5.14}$$

which yields the limiting values

$$\frac{\mathrm{d}\hat{t}^*}{\mathrm{d}x} = \begin{cases} \infty & \text{if } h'(\hat{T}) > -cx_0, \\ -\dfrac{1}{\hat{\Gamma}_0}\dfrac{h''(\hat{T})}{h'(\hat{T})^2} & \text{if } h'(\hat{T}) = -cx_0, \\ -\infty & \text{if } h'(\hat{T}) < -cx_0 \end{cases} \tag{5.15}$$

at $x = x_0$.

According to (5.15) the unsteady sonic line, therefore, starts at the downstream boundary $x = x_0$ if $h'(\hat{T}) \leqslant -cx_0$, while two branches propagating upstream and downstream are generated in an interior point $0 < x < x_0$ if $h'(\hat{T}) > -cx_0$.

As an example, the results summarized in this section have been evaluated numerically for the case that the imposed density distribution at $x = x_0$ is a linear function of time:

$$h(\xi) = -\frac{\xi}{\hat{T}}\rho_1^{sub}(x_0), \quad 0 \leqslant \xi \leqslant \hat{T}. \tag{5.16}$$

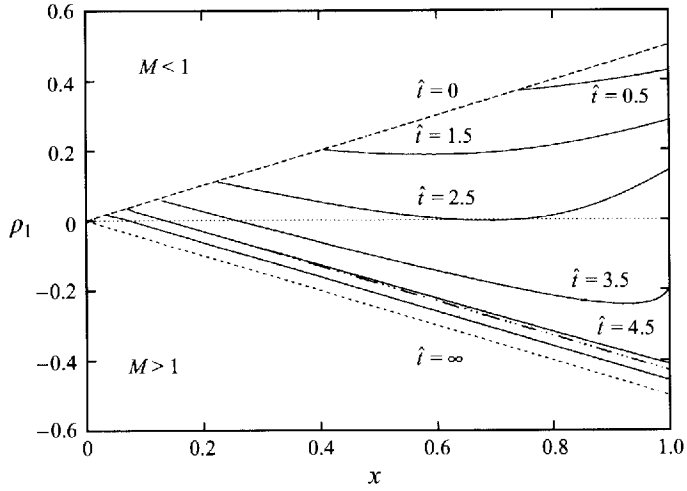

FIGURE 8. Laval nozzle: perfect gas for the same parameters as figure 7. Density distributions for various values of $\hat{t}$. -----, Initial density distribution and density distribution corresponding to steady accelerating flow; —···—, asymptotic relationship (5.18), $\hat{t} = 4.5$.

Figure 7 shows the location of characteristic curves and the unsteady sonic line in the $(x, \hat{t})$-plane. Initially the characteristics emanating from $x = x_0$, $0 \leqslant \xi \leqslant \hat{T}$ propagate upstream. On each of these characteristics, therefore, $A(x)$ decreases with increasing propagation time until the sonic state $\rho_1 = 0$ is reached at time $\hat{t} = \hat{t}^*(\xi)$. As the characteristic passes through the unsteady sonic line, the fluid enters the supersonic flow regime and, consequently, the characteristic starts to travel downstream and eventually leaves the region $x \leqslant x_0$ under consideration. With increasing time, therefore, the divergent part of the nozzle $0 \leqslant x \leqslant x_0$ only contains characteristics for which $|h(\xi)|$ is smaller than a time-dependent upper boundary $S(\hat{t})$ satisfying

$$|h(\xi)| < S(\hat{t}) \to 0 \quad \text{as} \quad \hat{t} \to \infty. \tag{5.17}$$

According to (5.6), however, $h(\xi)$ for $\hat{t} > \hat{t}^*(\xi)$ characterizes the deviations of the density perturbations from the supersonic solution, which thus is reached asymptotically in the limit $\hat{t} \to \infty$.

Density distributions in the divergent part of the nozzle $x \geqslant 0$ are depicted in figure 8 for various values of $\hat{t}$. Also, results for large values of $\hat{t}$ are compared with the asymptotic approximation

$$\rho_1(x, \hat{t}) \sim -\left(\frac{c}{\hat{\Gamma}_0}\right)^{1/2} [x - 2x_0 \exp(-\hat{t}(\hat{\Gamma}_0 c)^{1/2})], \tag{5.18}$$

which follows from (5.8), (5.9), (5.11) and (5.12) in the limit $\hat{t} \to \infty (\xi \to 0)$. Good agreement is observed except for a contracting region near the throat, where the assumption $\xi/x \ll 1$ made in the derivation of (5.18) is violated.

5.2. *Laval nozzle: BZT-fluid*

As shown in I, steady nozzle flows of BZT-fluids are qualitatively similar to those of perfect gases if $\hat{\Gamma}_0 > 3\hat{A}_0^2/8N_0$. Owing to the close relationship between the compatibility condition for steady and unsteady flows pointed out earlier (§3.3) this is true also for the start problem, which, therefore, will not be discussed in detail. Significant

deviations from the classical behaviour are observed, however, if $\hat{\Gamma}_0 \leqslant 3\hat{A}_0^2/8N_0$. Moreover, the results presented in I indicate that different forms of the unsteady responses are expected to occur in the parameter ranges $3\hat{A}_0^2/8N_0 > \hat{\Gamma}_0 > \hat{A}_0^2/3N_0$ and $\hat{A}_0^2/3N_0 > \hat{\Gamma}_0 > 0$. Although the flow properties in these parameter ranges are different for positive and negative values of $\hat{A}_0$ the following discussion is simplified by the fact that the nature of the transition process for $3\hat{A}_0^2/8N_0 > \hat{\Gamma}_0 > \hat{A}_0^2/3N_0$, $\hat{A}_0 > 0$ or $\hat{A}_0 < 0$ is qualitatively similar to that for $\hat{A}_0^2/3N_0 > \hat{\Gamma}_0 > 0$, $\hat{A}_0 < 0$ or $\hat{A}_0 > 0$. As a consequence, it is sufficient to study two typical cases with $\hat{A}_0 > 0$. To this end the system of governing equations consisting of the slope condition (3.20) and the compatibility condition (3.21*a*) was integrated numerically using a Runge–Kutta algorithm of sixth order.

Before turning to the specific problems it is important to note, that the shape of characteristic curves $\xi = \text{const.}$ in the $(x, \hat{t})$-plane qualitatively resembles the shape of the (j_1, ρ_1)-relationship if $\mathrm{d}A/\mathrm{d}x$ does not change sign in the x-domain under investigation. As an example, we consider a characteristic that carries a positive value of $\rho_1 = \rho_1^i > 0$ at the starting point $x = x^i, \hat{t} = 0$, say. Furthermore, we assume $\mathrm{d}A/\mathrm{d}x > 0$ and take into account that in the parameter range of interest the sonic values of the density satisfy

$$\rho_{1,3}^* < \rho_{1,2}^* < \rho_{1,1}^* = 0. \tag{5.19}$$

Owing to the assumption $\rho_1^i > 0$ the characteristic initially propagates upstream (figure 9). According to (3.21*a*) with $\mathrm{d}A/\mathrm{d}x > 0$ the density disturbance ρ_1 on the characteristic decreases monotonically with increasing time and, therefore, the sonic state $\rho_1 = \rho_{1,1}^* = 0$ is reached eventually at $\hat{t} = \hat{t}_1^*$. As ρ_1 passes through this critical value, the characteristic starts to move downstream with increasing speed. However, decreasing values of ρ_1 cause Γ to decrease also and finally to become negative. Inside the negative-Γ-regime a reduction of ρ_1 is associated with a reduction of the wave speed. Consequently, the characteristic decelerates until the fluid reaches the second sonic state $\rho_1 = \rho_{1,2}^*$ at $\hat{t} = \hat{t}_2^*$, which causes the propagation direction to change again. The characteristic travels upstream with increasing speed but the motion slows as the fluid finally returns into the positive-Γ-regime. Further decrease of the density disturbance ρ_1 then leads to the occurrence of the third sonic state $\rho_1 = \rho_{1,3}^*$ at $\hat{t} = \hat{t}_3^*$. For $\hat{t} > \hat{t}_3^*$ the characteristic moves downstream and eventually leaves the flow region under consideration.

Similar to §5.1 the parameterization $\xi = \hat{t}$ is adopted at $x = x_0$ and the imposed density perturbations are taken to vary linearly with time until the (first) sonic state $\rho_1 = \rho_{1,1}^* = 0$ is reached:

$$h(\xi) = -\frac{\xi}{\hat{T}_1}\rho_1^{sub}(x_0), \quad 0 \leqslant \xi \leqslant \hat{T}_1. \tag{5.20}$$

In order to avoid shocks which originate at the downstream boundary $h(\xi)$ for $\xi > \hat{T}_1$ is chosen such that the density disturbances following from (5.4) agree with the density disturbances on the characteristics generated at x_0 during the time interval $0 \leqslant \hat{t} \leqslant \hat{T}_1$. In contrast to the perfect gas case these characteristics exhibit three sonic points and, consequently, three unsteady sonic lines emanate from the downstream boundary at $\hat{t} = \hat{T}_1$, $\hat{t} = \hat{T}_2$, $\hat{t} = \hat{T}_3$ (in order to determine the function $h(\xi)$ for $\xi > \hat{T}_1$, therefore, the density variation on characteristics $0 \leqslant \xi \leqslant \hat{T}_1$ that leave the computational domain during $\hat{T}_1 \leqslant \hat{t} \leqslant \hat{T}_2$ but re-enter during $\hat{T}_2 \leqslant \hat{t} \leqslant \hat{T}_3$ and finally leave for $\hat{t} \geqslant \hat{T}_3$ has to be considered; for completeness the location of these characteristics

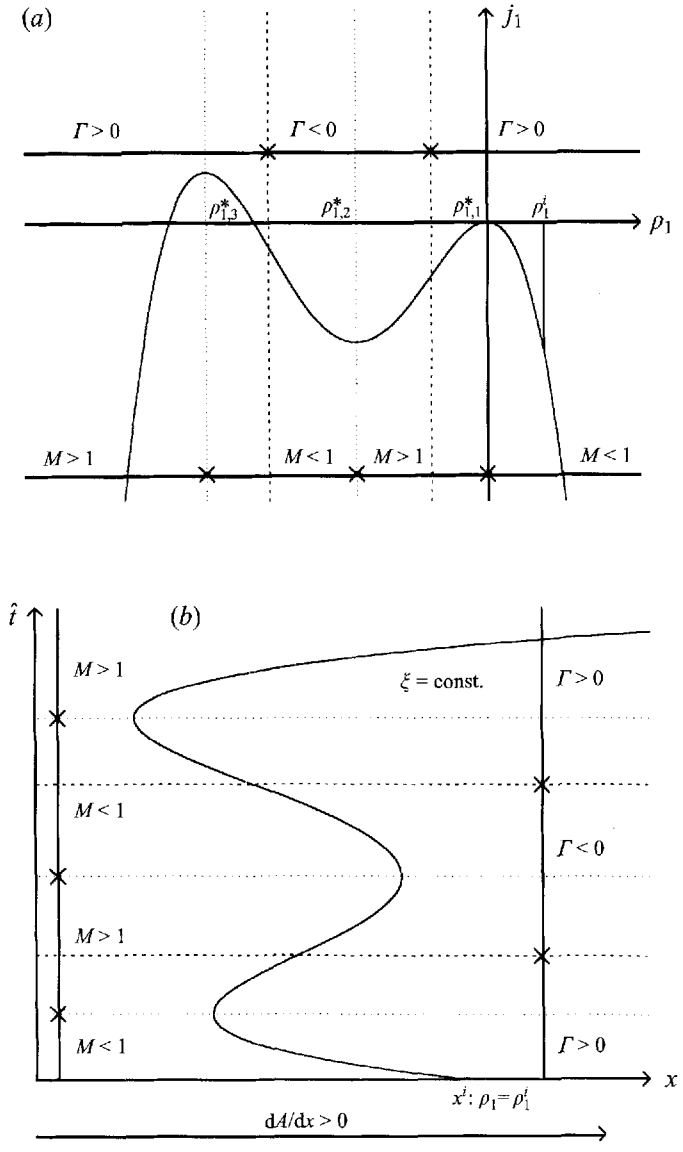

FIGURE 9. Correspondence between (*a*) the shape of the (j_1, ρ_1)-plot and (*b*) the shape of characteristic curves $\xi = \text{const.}$ in the $(x, \hat{t})$-plane for $dA/dx > 0$.

for $x > x_0$ is included in figure 10). The slopes of these sonic lines at $x = x_0$ can be calculated directly from (5.15) if $\hat{\Gamma}_0$ is replaced by the appropriate value

$$\hat{\Gamma} = \hat{\Gamma}_0 + \hat{A}_0 \rho_1 + \tfrac{1}{2} N_0 \rho_1^2, \quad \rho_1 = \rho^*_{1,i=1,2,3} \tag{5.21}$$

of the fundamental derivative.

Typical numerical results for the parameter range $3\hat{A}_0^2/8N_0 > \hat{\Gamma}_0 > \hat{A}_0^2/3N_0$, $\hat{A}_0 > 0$ are summarized in figures 10(*a*) and 11(*a*). As in the case of a perfect gas the unsteady sonic line $\rho_1 = 0$ does not reach the throat $x = 0$ in finite time and the flow properties in the converging part of the nozzle are not affected by the transition process. For this reason characteristic curves and density distributions are depicted for $x \geqslant 0$ only.

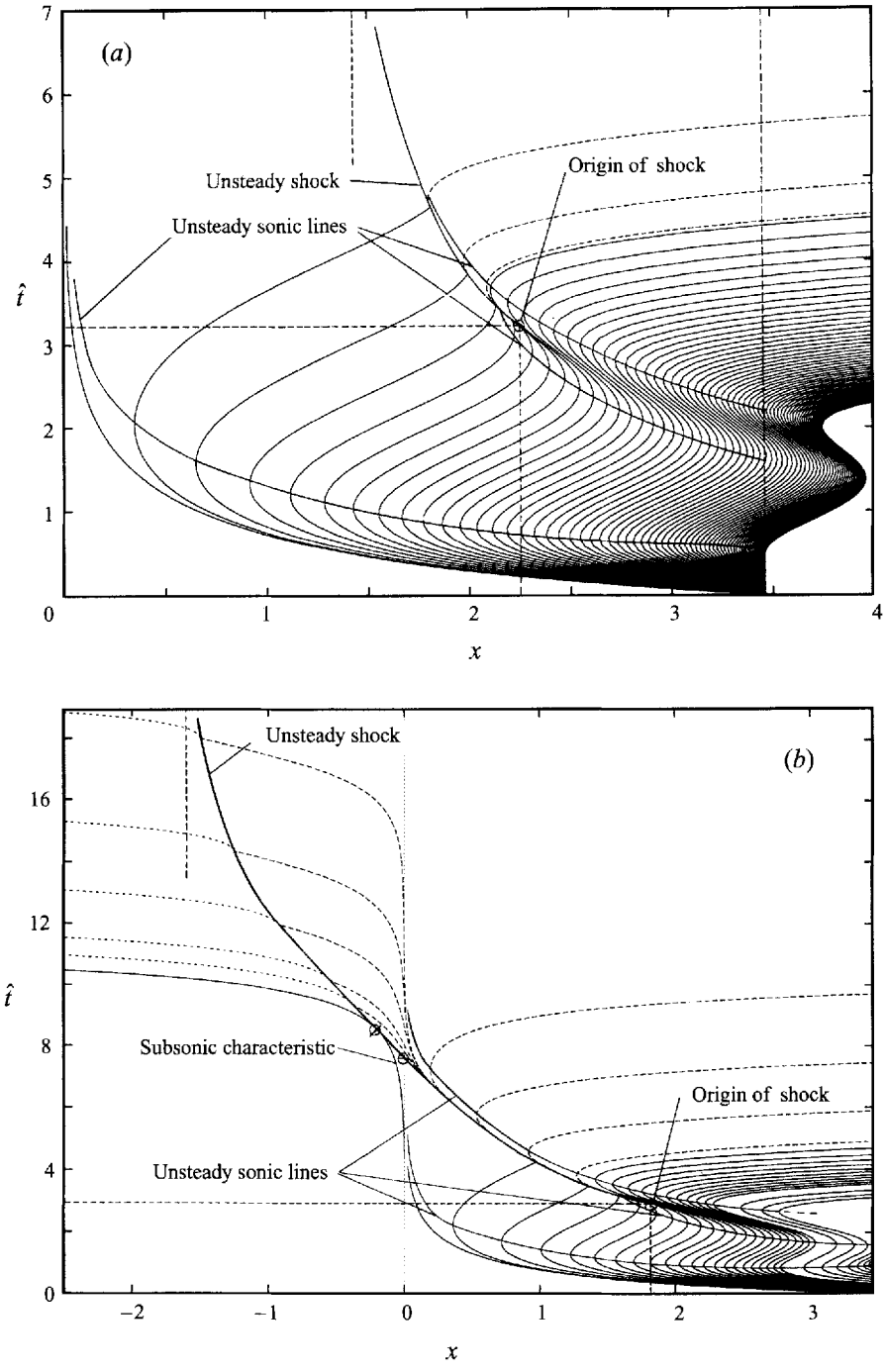

FIGURE 10. Laval nozzle: BZT-fluid with (*a*) $3\hat{A}_0^2/8N_0 > \hat{\Gamma}_0 > \hat{A}_0^2/3N_0$, $\hat{A}_0 > 0$ ($\hat{\Gamma}_0 = 4.91$, $\hat{A}_0 = 15.8$, $N_0 = 17.67$, $c = 0.3$, $x_0 = 3.46$, $\rho_1^{sub}(x_0) = 0.637$, $\hat{T} = 0.5 < \rho_1^{sub}(x_0)/cx_0 = 0.614$), and (*b*) $\hat{A}_0^2/3N_0 > \hat{A}_0 > 0$, $\hat{A}_0 > 0$ ($\hat{\Gamma}_0 = 3.48$, $\hat{A}_0 = 14.03$, $N_0 = 17.48$, $c = 0.3$, $x_0 = 3.46$, $\rho_1^{sub}(x_0) = 0.695$, $\hat{T} = 1 > \rho_1^{sub}(x_0)/cx_0 = 0.670$). Position of characteristic curves, unsteady sonic lines and the expansion shock in the $(x, \hat{t})$-plane. ——, Characteristics ξ emanating from the downstream boundary; -----, characteristics ξ emanating from the sonic portion of the expansion shock.

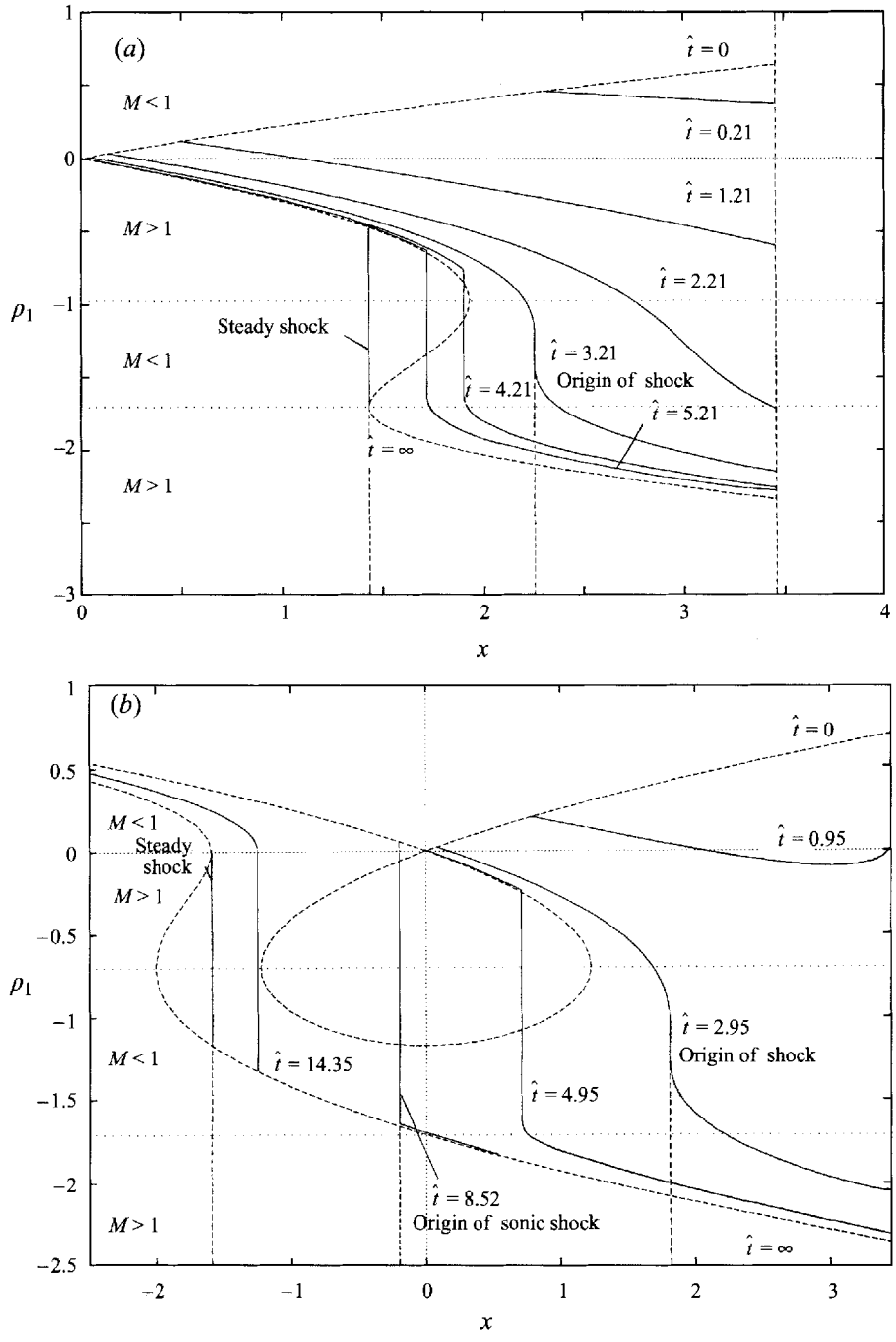

FIGURE 11. Laval nozzle; BZT-fluid with (*a*) $3\hat{A}_0^2/8N_0 > \hat{\Gamma}_0 > \hat{A}_0^2/3N_0$, $\hat{A}_0 > 0$ ($\hat{\Gamma}_0 = 4.91$, $\hat{A}_0 = 15.8$, $N_0 = 17.67$, $c = 0.3$, $x_0 = 3.46$, $\rho_1^{sub}(x_0) = 0.637$), and (*b*) $\hat{A}_0^2/3N_0 > \hat{\Gamma}_0 > 0$, $\hat{A}_0 > 0$ ($\hat{\Gamma}_0 = 3.48$, $\hat{A}_0 = 14.03$, $N_0 = 17.48$, $c = 0.3$, $x_0 = 3.46$, $\rho_1^{sub}(x_0) = 0.695$). Density distributions for various values of $\hat{t}$. -----, Initial density distribution and density distribution corresponding to steady accelerating flow.

A more detailed investigation shows the existence of an overlap region starting at a point located between the second and third sonic line where characteristic curves touch each other at the inflexion points $\Gamma = 0$. This leads to the formation of an expansion shock whose initial slope is given by

$$\hat{W} = \hat{W}(\rho_1^{in}) \quad \text{with} \quad \rho_1^{in} = -\frac{\hat{A}_0}{N_0}\left[1 \mp \left(1 - 2\frac{\hat{\Gamma}_0 N_0}{\hat{A}_0^2}\right)^{1/2}\right]. \tag{5.22}$$

This shock has a sonic downstream state (figure 10*a*) and thus generates additional characteristics, which for $\hat{t} \to \infty$, e.g. as the shock approaches its steady-state position, determine the density distribution downstream.

Density profiles for various values of $\hat{t}$ are plotted in figure 11(*a*). It is seen that the density distributions upstream and downstream of the expansion shock approach the steady flow solution much faster than the shock position.

Results for a typical case with $\hat{A}_0^2/3N_0 > \hat{\Gamma}_0 > 0$, $\hat{A}_0 > 0$ are displayed in figures 10(*b*) and 11(*b*). As in the case discussed above the reduction of the density/pressure at $x = x_0$ leads to the occurrence of an expansion shock whose origin coincides with the inflexion point of the characteristic that determines the cusp of an envelope. Initially, this shock has a sonic downstream state and, owing to its supersonic upstream conditions, the shock reaches the throat in finite time. As it passes through the throat, the shock becomes non-sonic again and starts to interact with the characteristics generated earlier during its first sonic phase. This interaction slows the shock and sonic upstream conditions are reached eventually. In this way a precursor region is generated, which in turn causes the necessary modifications of the density distribution upstream of this shock as it asymptotes its steady-state position in the limit $\hat{t} \to \infty$. Similar to figure 11(*a*) the shock position is found to approach its steady flow result much more slowly than the upstream and downstream density profiles.

5.3. *Nozzles with two throats*

As shown in I, BZT-fluids can be accelerated shock free by means of a classical Laval nozzle if $\hat{\Gamma}_0 > 3\hat{A}_0^2/8N_0$ only. If $\hat{\Gamma}_0 < 3\hat{A}_0^2/8N_0$ shock-free solutions leading from subsonic to supersonic flow conditions were shown to exist for specially tailored nozzles with two throats rather than a single throat. For example, a linear density/pressure distribution

$$\rho_1 = p_1 = -cx \tag{5.23}$$

can be achieved by means of the nozzle contour

$$A_4(x) = Q_{max} - j_1(-cx) = Q_{max} + \hat{\Gamma}_0(cx)^2 - \tfrac{1}{3}\hat{A}_0(cx)^3 + \tfrac{1}{12}N_0(cx)^4. \tag{5.24}$$

Here Q_{max} denotes the value of j_1 at the maximum of the (j, ρ_1)-relationship that defines the maximum value of the perturbation mass flux entering the steady flow version of the mass balance (3.23).

Only the solution corresponding to $Q = Q_{max}$ was considered in I. Density distributions for various values of Q are depicted in figure 12. As in § 5.2 it is sufficient to consider the cases $3\hat{A}_0^2/8N_0 > \hat{\Gamma}_0 > \hat{A}_0^2/3N_0$, $\hat{A}_0 > 0$ and $\hat{A}_0^2/3N_0 > \hat{\Gamma}_0 > 0$, $\hat{A}_0 > 0$.

Figure 12 reveals the important result that the solution of the steady flow problem with $Q = Q_{max}$ is non-unique. In addition to the desired shock-free expansion (5.23) there exists a second solution, which contains a sonic expansion shock located in the second throat (for $3\hat{A}_0^2/8N_0 > \hat{\Gamma}_0 > \hat{A}_0^2/3N_0$) or between the antithroat and the second throat (for $\hat{A}_0^2/3N_0 > \hat{\Gamma}_0 > 0$). As pointed out earlier, the formal solution of the compatibility condition (3.22) for unsteady flow differs from its steady counterpart (3.23) only insofar as the integration constant Q is replaced by a function of ξ. This

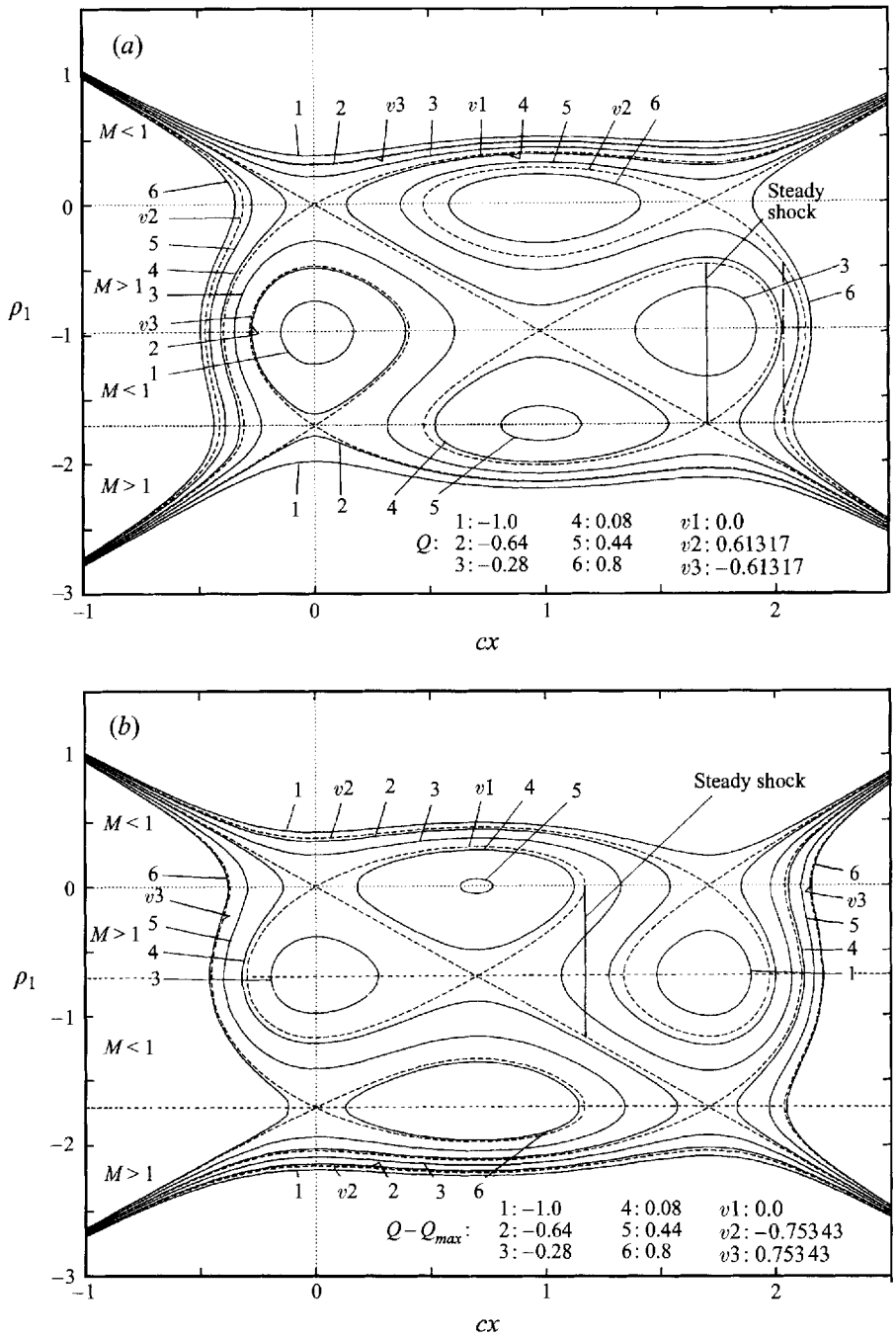

FIGURE 12. Nozzle with two throats: BZT-fluid with (*a*) $3\hat{A}_0^2/8N_0 > \hat{I}_0 > \hat{A}_0^2/3N_0$, $\hat{A}_0 > 0$ ($\hat{I}_0 = 4.91$, $\hat{A}_0 = 15.8$, $N_0 = 17.67$), and (*b*) $\hat{A}_0^2/3N_0 > \hat{I}_0 > 0$, $\hat{A}_0 > 0$ ($\hat{I}_0 = 3.48$, $\hat{A}_0 = 14.03$, $N_0 = 17.48$). Steady density distributions for various values of Q (linear distribution for $Q = Q_{max} = 0$ in (*a*) and $Q = Q_{max} = 0.7534$).

implies that – on each fixed characteristic $\xi = \text{const.}$ – j_1 and A_4 are related in exactly the same way as in the case of steady flow. As a result, we conclude that the portion of the steady distribution (5.23) located inside the loops branching off at the saddle points situated at the antithroat and the first or second throat, respectively, cannot be

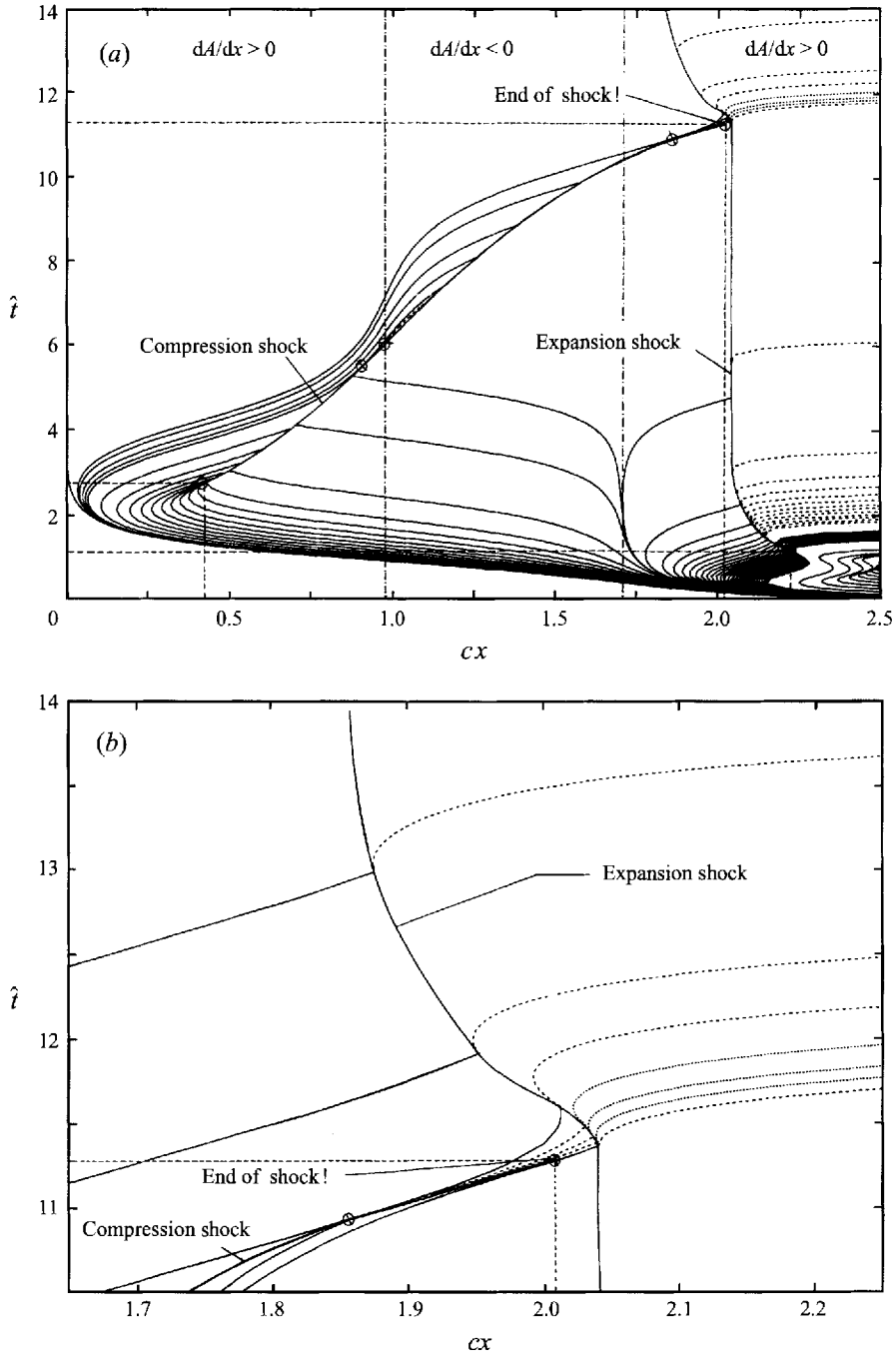

FIGURE 13. (*a*) Nozzle with two throats: BZT-fluid with $3\hat{A}_0^2/8N_0 > \hat{\Gamma}_0 > \hat{A}_0^2/3N_0$, $\hat{A}_0 > 0$ ($\hat{\Gamma}_0 = 4.91$, $\hat{A}_0 = 15.8$, $N_0 = 17.67$, $c = 0.5$, $x_0 = 5.0$, $\rho_1^{sub}(x_0) = 0.775$). Position of characteristics, unsteady sonic lines and the shocks in the $(x, \hat{t})$-plane. ——, Characteristics ξ emanating from the downstream boundary; -----, characteristics ξ emanating from the sonic portions of the shocks; ·····, characteristics ξ emanating from that sonic portion of the expansion shock which is formed by characteristics generated by the compression shock. (*b*) Detail of (*a*) showing the interaction zone of the compression and the expansion shock.

generated by characteristics emanating from the downstream boundary $x = x_0$. It thus appears that the steady solution with a sonic expansion shock rather than a shock-free solution will be realized by transition processes of the form investigated here.

As shown in figure 13 for the case $3\hat{A}_0^2/8N_0 > \hat{\Gamma}_0 > \hat{A}_0^2/3N_0$, $\hat{A}_0 > 0$, this conclusion is in excellent agreement with the numerical computations. Herein, starting with the steady solution $v1$ (figure 12*a*) having a subsonic state in the second throat, the density at the downstream boundary $x = x_0$ was lowered continuously until ρ_1 assumed the value corresponding to the purely accelerating linear solution given by (5.23). Since the flow properties upstream of the first throat $x = 0$ remain unaffected by the boundary conditions at $x = x_0$ for all times figure 13 is limited to the region $x \geqslant 0$ including the antithroat $x = -\rho^*_{1,2}/c$ and the second throat $x = -\rho^*_{1,3}/c$.

In the early stage of the transition process the flow in the second throat is still subsonic and characteristics with sufficiently small values of $\xi < \xi_0$, therefore, are able to pass upstream through this throat and also through the antithroat. On each of these characteristics critical flow conditions are attained before they can reach the first throat, however, and they are swept downstream as the density perturbations enter the supersonic regime. Since characteristics with smaller values of ξ propagate faster than those with larger values of ξ, they converge to generate a compression shock, which eventually evolves into a sonic shock but becomes non-sonic again at the time at which it passes through the antithroat. As a result, the characteristics shed by the sonic portion of the shock merge with the shock front at later time thus forming a closed pocket that does not influence the large-time behaviour of the flow properties significantly. In contrast, the characteristics generated during the second sonic phase of this shock initiated by its passage through the second throat are of essential importance as far as the approach to steady flow conditions in the limit $\hat{t} \to \infty$ is concerned. In order to see this it is necessary now to consider the time history of characteristics $\xi \geqslant \xi_0$ where the limiting characteristic $\xi = \xi_0$ is characterized by the property that a sonic state occurs at the throat in the limit $\hat{t} \to \infty$, with the starting value $\rho_1(x_0, \xi_0)$ corresponding to the upper branch of the steady solution $v2$ (figure 12*a*). Characteristics with $\xi > \xi_0$, therefore, turn back before they can reach the second throat and, as a consequence, the flow downstream of this throat evolves – on an intermediate timescale – in very much the same way as in the divergent part of a conventional Laval nozzle (figure 10*a*). In particular, an expansion shock is formed, which develops a sonic downstream state and approaches the position defined by the dotted line in figure 12(*a*). Eventually, however, this shock starts to interact with characteristics $\xi < \xi_0$ returning from the region between the first throat and the antithroat and the compression shock formed by these characteristics. In the case studied here the mechanism described first by Kluwick & Czemetschka (1990) causes this shock to terminate a short distance upstream of the expansion shock (figure 13*b*). The interaction process between the characteristics shed by the second, terminating sonic portion of this shock, the characteristics $\xi < \xi_0$ downstream of this shock and the sonic expansion shock leads to an acceleration of the latter in the upstream direction. As the expansion shock is pushed upstream, its strength decreases only slightly and it finally asymptotes the position of the shock present in the second steady flow solution with $Q = Q_{max}$.

6. Conclusions

The start problem of nozzle flow in the dense-gas regime involves the interesting question whether and how information can propagate upstream from the nozzle exit

through multiple sonic states. In order to gain some insight into this problem we consider a simplified transonic version, e.g. we consider the transient motion that sets in if a steady subsonic solution is perturbed by lowering the pressure continuously at some fixed position $x = x_0$ until the value corresponding to a subsonic–supersonic expansion is reached. To this end the modified viscous transonic small-perturbation equation for steady flow derived in I is generalized to include the effect of upstream-propagating waves. As in I the calculations are based on the standard Navier–Stokes equations supplemented with a non-standard equation of state which accounts for the fact that the Mach number density relationship of a BZT-fluid may exhibit three sonic states rather than a single one.

For simplicity it is assumed that the initially imposed steady subsonic solution reaches a sonic state at the throat or at one of the throats if the nozzle has two constrictions. Cases where the initial distribution of the field variables is purely subsonic can also be treated, in principle. However, since the variation of the flow quantities on each fixed wavelet is of exactly the same form as in the case of steady flow, transient flows of the latter type are not expected to yield qualitatively new results. Most important, they are subject to the same difficulty encountered in the problems studied here, namely that upstream-propagating wavelets do not reach a sonic throat in finite time.

In both cases investigated in the present paper this difficulty is resolved by the formation of an expansion shock inside the expansion wave generated downstream of the throat, which initially has a supersonic upstream state. This ensures that information can propagate upstream from $x = x_0$, where the expansion wave is initiated, to a sonic throat in finite time.

In addition the results obtained indicate that a shock-free subsonic–supersonic expansion in a nozzle with two throats cannot be obtained by the kind of transition process considered here. A more detailed examination of the steady flow problem shows that the solution leading from a subsonic to a supersonic state is indeed non-unique. In addition to the desired shock-free solution there exists a second solution with an embedded shock discontinuity. It is this solution that represents the steady-state limit of the unsteady transition process. It would be interesting to know whether this result remains valid if two-dimensional effects are accounted for. If so, this would have important consequences for the design of shock-free cascades which is one of the most intriguing possibilities of dense-gas dynamics.

REFERENCES

ADAMSON, T. C. JR & MESSITER, A. F. 1988 Asymptotic methods for internal transonic flows. *Transonic Symposium; Theory, Application and Experiment, NASA Conf. Publ.* 3020, vol. 1, pp. 261–291.

ADAMSON, T. C. JR, MESSITER, A. F. & RICHEY, G. K. 1974 On the matching of solutions for unsteady transonic nozzle flows. *Arch. Mech. Stosow* **26**, 617–628.

ADAMSON, T. C. JR & RICHEY, G. K. 1973 Unsteady transonic flows with shock waves in two-dimensional channels. *J. Fluid Mech.* **60**, 363–382.

ANGELINO, G. & INVERNIZZI, C. 1993 Cyclic methylsiloxanes as working fluids for space power cycles. *J. Solar Engng* **115**, 130–137.

BETHE, H. A. 1942 The theory of shock waves for an arbitrary equation of state. *Office Sci. Res. Dev. Rep.* 545.

BURNSIDE, B. M. 1973 Thermodynamic properties of five halogenated hydrocarbon vapour cycle working fluids. *J. Mech. Engng Sci.* **15**, 132–143.

CHANDRASEKAR, D. & PRASAD, P. 1991 Transonic flow of a fluid with positive and negative nonlinearity through a nozzle. *Phys. Fluids* A **3**, 427–438.

CRAMER M. S. 1991 Nonclassical dynamics of classical gases. In *Nonlinear Waves in Real Fluids* (ed. A. Kluwick), pp. 91–145. Springer.

CRAMER, M. S. & CRICKENBERGER, A. B. 1991 The dissipative structure of shock waves in dense gases. *J. Fluid Mech.* **223**, 325–355.

CRAMER, M. S. & FRY, R. N. 1993 Nozzle flows of dense gases. *Phys. Fluids* A **5**, 1246–1259.

CRAMER, M. S. & KLUWICK, A. 1984 On the propagation of waves exhibiting both positive and negative nonlinearity. *J. Fluid Mech.* **142**, 9–37.

CRAMER, M. S. & TARKENTON, G. M. 1992 Transonic flows of Bethe–Zel'dovich–Thompson fluids. *J. Fluid Mech.* **240**, 197–228.

CURRAN, H. M. 1981 Use of organic working fluids in rankine engines. *J. Energy* **5**, 218–223.

KLUWICK, A. 1972 Schallnahe Wellenausbreitungsvorgänge in schlanken Düsen. *Acta Mechanica* **15**, 105–119.

KLUWICK, A. 1991 Small-amplitude finite-rate waves in fluids having both positive and negative nonlinearity. In *Nonlinear Waves in Real Fluids* (ed. A. Kluwick), pp. 1–43. Springer.

KLUWICK, A. 1993 Transonic nozzle flow of dense gases. *J. Fluid Mech.* **247**, 661–688 (referred to herein as I).

KLUWICK, A. & CZEMETSCHKA, B. 1990 Kugel- und Zylinderwellen in Medien mit positiver und negativer Nichtlinearität. *Z. Angew. Math. Mech.* **70**, 207–208.

MESSITER, A. F. & ADAMSON, T. C. JR 1975 On the flow near a weak shock wave downstream of a nozzle throat. *J. Fluid Mech.* **69**, 97–108.

OSWATITSCH, K. & ROTHSTEIN, W. 1942 Das Strömungsfeld in einer Laval-Düse. *Jb. Dtsch. Lufo.* **I**, 91–102.

RYSHOV, O. S. 1967 *Zh. Vychisl. Mat. Mat. Fyz.* **7**, 859–866. Engl. transl: Operation of laval nozzles in undesigned [i.e. off-design] modes. *USSR Comp. Math. Math. Phys.* **7**, No. 4, 187–195.

RYZHOV, O. S. 1978 Viscous transonic flows. *Ann. Rev. Fluid Mech.* **10**, 65–92.

SMITH, I. K. 1981 The choice of working fluids for power recovery from waste heat streams. *Paper* C70, *Trans. Conf. on Organic Fluids for Waste Recovery in Ships and Industry, London.*

SZANIAWSKI, A. 1965 Transonic approximations to the flow through a nozzle. *Arch. Mech. Stosow* **17**, 79–85.

THOMPSON, P. A. 1971 A fundamental derivative in gasdynamics. *Phys. Fluids* **14**, 1843–1849.

THOMPSON, P. A. 1991 Liquid-vapour adiabatic phase changes. In *Nonlinear Waves in Real Fluids* (ed. A. Kluwick), pp. 147–213. Springer.

THOMPSON, P. A. & LAMBRAKIS, K. C. 1973 Negative shock waves. *J. Fluid Mech.* **60**, 187–207.

TOMOTIKA, S. & TAMADA, K. 1950 Studies on two-dimensional transonic flows of compressible fluids – Part I. *Q. Appl. Maths* **7**, 381–397.

WHITHAM, G. B. 1974 *Linear and Nonlinear Waves.* John Wiley and Sons.

ZEL'DOVICH, YA. B. 1964 On the possibility of rarefaction shock waves. *Zh. Eksp. Teor. Fiz.* **4**, 363–364.

ZÖRNER, W. & BLUMENBERG, J. 1989 Der Organische Rankine-Prozeß zur solardynamischen Energieerzeugung im Weltraum. *Z. Flugwiss. Weltraumforsch.* **13**, 260–270.